Mechanics of Materials 140 (2020) 103219

Contents lists available at ScienceDirect

Mechanics of Materials

journal homepage: www.elsevier.com/locate/mechmat

Research paper

Towards exploiting inelastic design for Inconel 625 under short-term cyclic loading at 600°C

I. Soner Cinoglu*, Ali Charbal, Natasha Vermaak

Department of Mechanical Engineering & Mechanics, Lehigh University, Bethlehem, PA, 18015, USA

ARTICLE INFO

Keywords:
Inconel 625
Alternating plasticity
Shakedown
Inelastic design
Elastoplastic behavior
Thermomechanical testing

ABSTRACT

Many industries rely on the Inconel 625 alloy to serve under thermomechanical operating conditions. Understanding the macroscopic cyclic inelastic behavior of this material is vital for accurate assessment of its load-carrying capacity at elevated temperatures. In this work, a uniaxial experimental program at 600°C is conducted to demonstrate designing for cyclic elastoplastic behavior (shakedown) as opposed to more restrictive first-yield, while still avoiding ratchetting or alternating plasticity. In particular, a range of cyclic stress amplitudes are imposed at non-zero mean stresses while maintaining a constant maximum stress. In addition, the effect of dynamic strain aging (DSA) on the macroscopic shakedown behavior is established under load control. The inelastic work done per cycle is used as a measure of severity of the cyclic inelastic behavior, and is evaluated by monitoring the evolution of the hysteresis loop width. It is found that when the maximum stress is constant, larger mean stress tests approach shakedown behavior. Furthermore, for the range of stress amplitudes and mean stresses considered, the cyclic elastoplastic shakedown behavior is not affected by the DSA, and only depends on the mean stress and stress amplitude.

1. Introduction

The nickel-based superalloy Inconel 625 (IN625) has been primarily used in aerospace, pressure vessel, marine, and gas turbine applications. The material is preferred in these applications for its high strength, corrosion resistance and creep resistance at elevated temperatures up to about 1140 °C (2100 °F) (Eiselstein and Tillack, 1991; Shoemaker, 2005; Rakowski et al., 2005; Thomas and Tait, 1994; Donachie and Donachie, 2002; Mankins and Lamb, 1990). Often the service conditions for this material involve complex cyclic thermomechanical loadings, and in some cases, such as hypersonic flight, could involve relatively few cycles. Conventionally, first-yield based methods are used for the design of aerospace structures to avoid plastic behaviors that lead to failure. However, design methods based on purely linear elastic behavior may also fail to find feasible or lightweight solutions. Thus, inelastic analysis (for shakedown) may be required to accurately assess the load-bearing capacity of thermostructural components.

Shakedown is a cyclic elastoplastic behavior in which local inelastic strains develop in the initial cycles, but the cyclic accumulation of plastic deformation is arrested upon further cycling. Shakedown behavior may be used as a design criterion against inadmissible cyclic inelastic behaviors (ratchetting and alternating plasticity). Ratchetting is the continued accumulation of plastic strain during cycling that leads to incremental collapse or rupture (Park et al., 2007; Zhu et al., 2017). In the case of alternating plasticity, an equal magnitude of plastic strain is obtained during the loading and unloading portions of each cycle, but with opposite sign (Suave et al., 2016; Algarni et al., 2017). As a result there is no net plastic strain increment but this behavior leads to failure due to low-cycle-fatigue (LCF). As local inelastic strains are allowed in shakedown-based designs, this method could be used when conventional yield-limited design methods are not feasible, especially at elevated temperatures (Heiser and Pratt, 1994; Klock and Cesnik, 2015). Shakedown based designs have been used in the nuclear industry for pressure vessels, but use in other industries is limited (Weichert and Ponter, 2014; Vermaak et al., 2018). One reason for this is the lack of available experimental demonstrations of shakedown behavior that will convince designers to adopt shakedown criteria as a safe-state beyond first-yield.

Inelastic shakedown-based design methods require load-contolled tests to determine safe loading limits to achieve shakedown behavior. In contrast, the cyclic inelastic behavior of IN625 has mostly been investigated through strain-controlled tests for low-cycle-fatigue (LCF) life (Bui-Quoc et al., 1988; Suave et al., 2016; Nagesha et al., 2012). In this way, there is a lack of studies investigating the material's behavior under force-controlled conditions in the literature. As one notable

* Corresponding author.
E-mail address: isc214@lehigh.edu (I.S. Cinoglu).

https://doi.org/10.1016/j.mechmat.2019.103219
Received 31 August 2019; Accepted 22 October 2019
Available online 24 October 2019

exception, the cyclic inelastic behavior of IN625 was investigated under both strain-controlled and force-controlled conditions by Suave et al. (2016). In particular, the authors study the effect of age hardening on the mechanical properties, low cycle fatigue, and ratchetting response as well as microstructural changes during cyclic loading at elevated temperatures. They concluded that age hardening improves the LCF performance due to strengthening by γ″ precipitate formation. They also observed that age hardening results in lower ratchetting rates.

Understanding interactions between cyclic plastic behaviors and rate-dependent behaviors such as dynamic strain aging (DSA) is of great importance to develop more robust design strategies. The effect of DSA on the material's behavior in load-controlled tests in the inelastic regime is also unknown. Based on strain/deformation based data, IN625 shows DSA behavior at a wide range of temperatures (250–750°C) and strain rates (10^{-5}–10^{-3} $1/s$) (Shankar et al., 2004; Kim and Chaturvedi, 1987; Chatterjee et al., 2015; de Oliveira et al., 2019). DSA is a strengthening mechanism caused by solute atoms that restrict dislocation movement in the microstructure. DSA results in rapid fluctuations (serrated yielding) in the macroscopic stress-strain behavior. It has been observed through a set of tensile tests that the critical strain for the onset of DSA for IN625 decreases with temperature and increases with strain rate in the temperature range of 250–450°C (Shankar et al., 2004; Kim and Chaturvedi, 1987). Above 450°C, the effects of temperature and strain rate on the critical DSA strain are not as clear. In addition to standard tensile tests, Maj et al. performed high-speed compression tests on IN625 at strain rates of 0.1, 1, and 10 s^{-1} at 600°C (Maj et al., 2017). They observed serrated yielding effects (an indicator for DSA) even at the largest strain rate in compression. To the best of the authors' knowledge, this paper is the first to present macroscopic shakedown and the effect of DSA on the cyclic inelastic stress-strain behavior of IN625 under force-control at 600°C.

In this paper the intent is to motivate inelastic design strategies (that could be used for example, to support hypersonic flight) by demonstrating macroscopic shakedown behavior for IN625 at 600°C in the presence of rate-dependent behaviors (DSA). In Section 2, details of the material used, sample preparation, and testing equipment are presented. Testing methods used in this study are described in Section 3. Experimental results and discussion are presented in Section 4, followed by conclusions.

2. Material and equipment

The chemical composition of the IN625 alloy used in this study is given in Table 1. Twelve inch cylindrical rods of 1 inch diameter were solution annealed at 1010°C and water quenched for 1 h. The rods were machined to achieve a test geometry based on ASTM standards E8, A370, and E466, as shown in Fig. 1 (Standard, 2004; 2005; 2002).

Following the machining, the surface between the gripping section of the samples was degreased and painted with a black and white speckle pattern using a spray paint (VHT FlameProof Coating) to be used for strain measurements by digital image correlation (DIC). After a drying period, the paint on the sample surfaces was cured following the supplier instructions. A curing cycle included heating the samples to an elevated temperature, soaking at this temperature for 30 min, and then cooling down for 30 min. Three curing cycles were applied at increasing temperature levels of 121 °C, 204 °C and 315 °C (250°F, 400°F, and 600°F).

Mechanical properties of the material such as the linear elastic limit

Table 1
Chemical composition of the material.

%C	%P	%Si	%Ni	%Ti	%Mn	%S	%Cr	%Mo	%Al
0.04	0.003	0.06	60.79	0.22	0.05	0.001	22.31	8.70	0.18

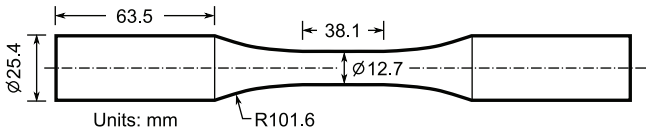

Fig. 1. Dimensions of the samples used for uniaxial tests in this study.

Table 2
Mechanical properties of the material at 600°C.

σ_y^o	$\sigma_y^{0.2\%}$	$\sigma_{cut-off}^{2\%}$	$\sigma_{cut-off}^{3\%}$
362 ± 17 MPa	473 ± 6 MPa	516 ± 4 MPa	550 ± 7 MPa

(σ_y^o), 0.2% yield limit ($\sigma_y^{0.2\%}$), 2% cut-off limit ($\sigma_{cut-off}^{2\%}$), and 3% cut-off limit ($\sigma_{cut-off}^{3\%}$) were determined as the average of three monotonic uniaxial tests in strain-control at 600°C, (Table 2). The linear elastic limit and 0.2% yield limit of the material was found to be the same in tension and compression. It was assumed that 2% and 3% cut-off limits are also the same. The tests were performed up to a 5% strain (approaching collapse) and at various strain rates from $3{\cdot}10^{-5}$ - $3{\cdot}10^{-3}$ s^{-1}. The maximum of 5% strain was also chosen in order to protect the extensometer used for strain measurements. As maximum accumulated inelastic strain is restricted by many design standards, 2% and 3% cut-off limits were included in Table 2. In this way, the cut-off limits represent the allowable stress for a maximum cut-off strain level (2% or 3%) that could be used for the design of structures. The equipment and methods for the monotonic uniaxial tests are described more below and in Section 3.2.

2.1. Test equipment

A MTS 319.25 servo-hydraulic axial-torsional testing frame with an axial load capacity of 250 kN (55 kip) was used for all of the mechanical testing. Hydraulic grips with 1 in. diameter were used to clamp cylindrical samples. During thermal and mechanical phases of the tests, rotational movement of one of the grips was free so that a zero torsional load was obtained on the samples. The testing frame was equipped with an Ambrell 6 kW induction heating system for the isothermal tests at 600°C. An induction coil was designed to ensure visibility of the gage section of the samples during the tests for non-contact DIC measurements. The induction system provides rapid heating and consistent heat production throughout the isothermal tests.

Strain measurements were performed using two different methods. A high-temperature, axial-only, MTS 632.53E-11 extensometer with a 1-inch gage length was used to measure axial strains in the gage section of the samples. Strain signal from this extensometer was also used to control the servo-hydraulic testing frame during monotonic and strain-controlled cyclic tests. No cooling of the extensometer was required as the extensometer is rated for accurate strain measurements up to 650 °C without cooling. The contact extensometer was accompanied by a stereo DIC system coupled with an infrared camera for full-field, non-contact measurements of temperature and thermomechanical strain fields on the sample surfaces in the gage section. As the testing temperature is close to the maximum temperature allowed for the use of the contact extensometer without cooling, a virtual extensometer that is available in the DIC software was used for comparison with the physical MTS extensometer readings to ensure that heat produced during the tests did not affect the measurement accuracy. The stereo DIC system was also equipped with a FLIR A655 infrared camera for temperature field measurements. The emissivity value used in the thermography software was calibrated by placing K-type Omega thermocouples on the sample and comparing with the non-contact measurements. In this way, full-field measurements of strain and temperature were taken with the DIC and thermal imaging equipment throughout all of the tests

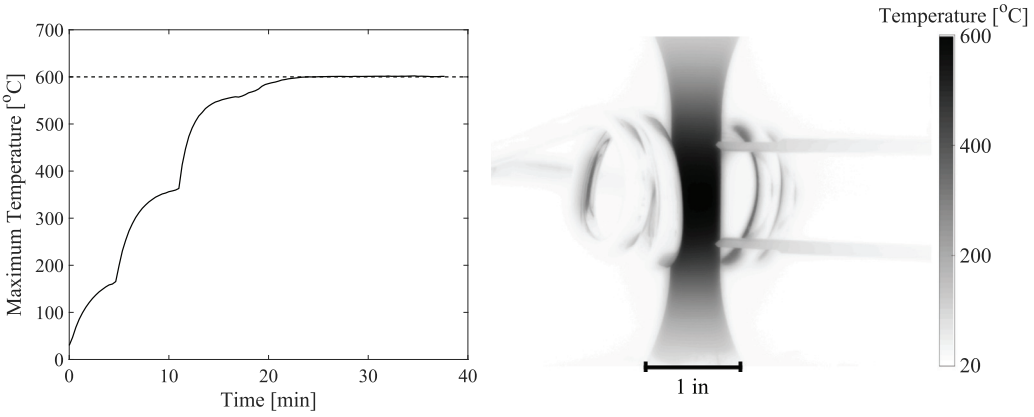

Fig. 2. a) Variation of the maximum temperature in the gage section and b) a representative thermal field after a 30 minute thermal soak for stabilization and before the mechanical tests were initiated.

presented below.

Using this equipment, the samples were heated until a maximum reading of 600˚C was achieved in the gage section, and then soaked for 20–30 min. for thermal stabilization before each thermomechanical test was initiated. Representative plots of maximum temperature and the change in thermal strain with time during heating as well as the temperature distribution after thermal stabilization are shown in Fig. 2a and b, respectively. It was found from the IR measurements that the target of 600˚C was typically achieved within 10 degrees (590˚C) or $< 1.6\%$ for the middle third of the gage section and 530˚C or $< 12\%$ for the gage extremities.

3. Experimental methods

Mechanical tests at 600˚C were performed on IN625 samples in strain-control (for monotonic tests) and force-control (for cyclic tests) modes. The tests were used to determine baseline properties, rate-dependency, and the cyclic inelastic response. The methods for each of these tests are described in the following.

3.1. Force-controlled cyclic test methods

Force-controlled cyclic tests were performed in order to establish whether or not shakedown states were achieved for a variety of cyclic tension-compression loading levels with non-zero mean stresses, listed in Table 3. In these tests, samples were first loaded to a non-zero mean stress (Fig. 3). Then, the stress was cycled with a predetermined amplitude; the loading rate was fixed at 15 MPa/s. The mean stress and stress amplitude levels (Table 3) were set such that the stress state in each sample would exceed the 0.2% yield stress ($\sigma_y^{0.2\%}$, Table 2) of the material during both loading and unloading for each cycle. This behavior is expected to cause ratchetting or alternating plasticity at large amplitudes and is illustrated schematically in Fig. 4. Note that each sample was tested at three stress amplitudes (for example, 1a, 1b, 1c, Table 3) while the mean stress on the sample was kept constant, as shown in Fig. 3. The purpose of testing one sample at multiple levels was to reduce the cost and time for testing (following cyclic plasticity procedures presented in Chaboche and Lemaitre, 1990). It will be shown later in Section 4.2, that performing these tests with consecutively increasing load levels on a single sample is negligably different from individual tests on separate samples (Chaboche and Lemaitre, 1990).

This procedure was used to investigate various mean stresses ranging from tension to compression. In order to facilitate comparison, when the mean stress was changed from tensile to compressive, the stress amplitude was set such that the maximum absolute stress on the samples stayed the same (Table 3). Repeatability was established by

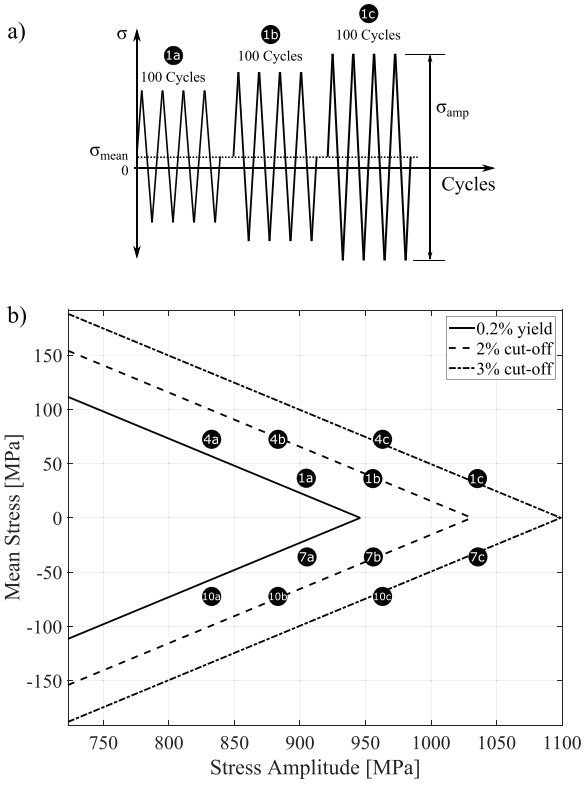

Fig. 3. a) Tension compression cycles applied in force-controlled cyclic experiments, b) load-interaction diagram showing the range of force-controlled cyclic tests from Table 3.

testing additional samples under the same loading conditions (samples #2, #5, #6, #8, and #11 are marked by "(r)" for repetition in Table 3). During all tests, 100 cycles were applied for each loading case (a, b or c). Also, one sample was tested directly at the largest stress amplitude for some of the mean stress cases (samples #3, #9, and #12 are denoted "single-level" in Table 3) to check if there was any effect of the prior cycles at smaller stress amplitudes on the behavior during the subsequent load levels (history effect).

In order to better visualize the testing program from Table 3, it is also presented in a load-interaction diagram in Fig. 3b. 0.2% yield ($\sigma_y^{0.2\%}$), 2% strain and 3% strain cut-off limits ($\sigma_{cut-off}^{2\%}$, $\sigma_{cut-off}^{3\%}$) are superimposed on the load-interaction diagram with the values given in Table 2. The limits of the load-interaction diagram are set such that all of the loading combinations shown cause yielding in both tension and compression. In particular, minimum and maximum limits of the stress

Table 3
Cyclic tests performed in force control. All stress values are in MPa.

Sample	Description (r: repetition)	Mean Stress [MPa]	Stress Amplitude			Maximum Stress		
			a	b	c	a	b	c
1	Multilevel	36	905	956	1035	489	514	554
2	Multilevel (r)	36	905	956	1035	489	514	554
3	Single-level	36	1035			554		
4	Multilevel	72	833	883	963	489	514	554
5	Multilevel (r)	72	833	883	963	489	514	554
6	Multilevel (r)	72	833	883	963	489	514	554
7	Multilevel	-36	905	956	1035	-489	-514	-554
8	Multilevel (r)	-36	905	956	1035	-489	-514	-554
9	Single-level	-36	-1035			-554		
10	Multilevel	-72	833	883	963	-489	-514	-554
11	Multilevel (r)	-72	833	883	963	-489	-514	-554
12	Single-level	-72	963			-553.9		

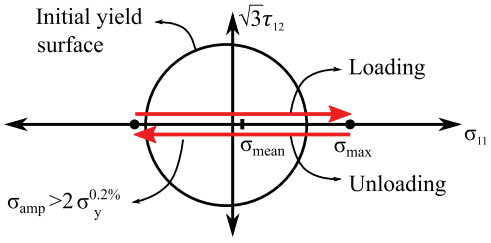

Fig. 4. An example of stress conditions in the first cycle of the force-controlled cyclic tests that would lead to ratchetting or alternating plasticity.

amplitude along the x-axis are set to $2{\cdot}\sigma_y^0 = 740$ *MPa* and $2{\cdot}\sigma_{cut-off}^{3\%} = 1100$ *MPa* to ensure plastic deformation at the minimum and maximum stresses reached during a cycle without exceeding the 3% strain cut-off limit of the material. Mean stress limits along the y-axis are bounded by the condition that the maximum stress should not exceed the 3% strain cut-off limit. The data points in Fig. 3b indicate the loading sets used in the testing program, Table 3. While the cyclic force-controlled tests can be used to establish shakedown, ratchetting or alternating plasticity responses, strain-controlled tests are also required in order to investigate the influence of the DSA behavior (which has been shown to be rate-dependent for IN625 Shankar et al., 2004; Kim and Chaturvedi, 1987) on the cyclic inelastic responses observed.

3.2. Monotonic strain-controlled tests for rate-dependent DSA behavior

Three monotonic tests were performed at 600°C in strain control using the MTS extensometer and FlexTest 40 controller. The results of these monotonic tests were used to report the properties in Table 2. The first test was at $\dot{\epsilon} = 3{\cdot}10^{-5}s^{-1}$, the second at $\dot{\epsilon} = 3{\cdot}10^{-4}s^{-1}$, and the last test used multiple rates: $3{\cdot}10^{-5}$, $3{\cdot}10^{-4}$, and $3{\cdot}10^{-3}s^{-1}$. For the multiple-rate test, the strain rate was incrementally increased and decreased to check the strain rate history effect. All three tests went up to a 5% maximum strain, approaching collapse, but limited in order to protect the extensometer.

4. Experimental results and discussion

4.1. Monotonic strain-controlled test results for rate-dependent DSA behavior

Strain-controlled monotonic test results from the three tests are shown in Fig. 5. The axial stress-strain responses in this figure correspond to the multi-rate test $\dot{\epsilon} = 3{\cdot}10^{-5}$, $3{\cdot}10^{-4}$ s^{-1}, and $3{\cdot}10^{-3}$ s^{-1} (black dots), the test at a constant rate of $\dot{\epsilon} = 3{\cdot}10^{-5}$ s^{-1} (red dots) and the one at $\dot{\epsilon} = 3{\cdot}10^{-4}$ (blue dots), respectively. The linear elastic limit (σ_y^o), 0.2% yield limit ($\sigma_y^{0.2\%}$), 2% cut-off limit ($\sigma_{cut-off}^{2\%}$), and 3% cut-off limit ($\sigma_{cut-off}^{3\%}$) given in Table 2 are superimposed on the stress-strain curves in Fig. 5 as horizontal dashed lines. These limits are useful to compare with the strain levels obtained in the force-controlled tests in Section 4.2.

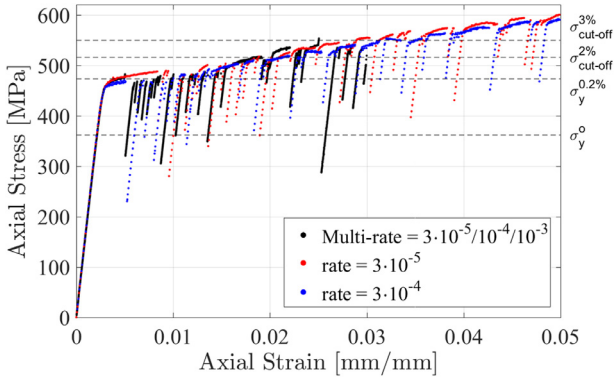

Fig. 5. Monotonic test results at 600°C.

These monotonic tests at different strain rates show that the rate-dependency of the mechanical properties is negligible. Dynamic strain aging behavior (serrated yielding) was observed at all of the strain rates used in these tests. The amplitude of the serrations in the monotonic tests vary widely; however, the critical strain at the onset of serrations decreased with the strain rate. For example, the DSA started at larger strain levels when the strain rate was the smallest ($\dot{\epsilon} = 3{\cdot}10^{-5}$). The implication is that DSA may be in effect at a wide range of rates (e.g. $10^{-5} - 10^{-3}$) and may start at very small strains in the force-controlled tests if the rate is greater than the fastest rate used in the monotonic tests ($\dot{\epsilon}_{max} = 3{\cdot}10^{-3}$).

4.2. Force-controlled cyclic test results at non-zero mean stress to characterize cyclic inelastic behavior

Fig. 6 shows results of the force-controlled cyclic tests from test #1, #3, and #4 in Table 3. A representative cyclic stress-strain response of a sample tested under a constant mean stress and three consecutively increasing stress amplitudes (test #1a in light gray, 1b in dark gray, and 1c in black) is shown in Fig. 6a. The maximum stresses reached at each cycle and at all three stress amplitude levels (see test method schematic in Fig. 3a) are given in Fig. 6b as a function of the cycle number. Similarly, representative stress-strain and peak-stress evolution results for sample #4 and sample #3 are shown in Figs. 6c-f. Line colors in these figures indicate the loading level (e.g. 4a in light gray, 4b in dark gray, 4c in black are the three stress amplitude levels applied on sample #4 (Table 3), as shown schematically in Fig. 3a. Note that sample #3 is a single-level test corresponding to the largest stress amplitude in the multi-level sample #1c but without the loading history (Table 3).

For Figs. 6 a, c, and e, at each stress amplitude level and during each cycle, the sample yields in both tension and compression, resulting in hysteresis loops. The loading levels were chosen in order to elicit this yielding and produce these hysteresis loops. Figs. 6b, d, f show that the maximum strains stabilize at all loading levels for samples 1, 3, and 4. In fact, this was the case for all of the tests listed in Table 3. This indicates that there is no net accumulation of plastic strain upon cycling (no ratchetting), and the relevant cyclic plastic behavior observed in the tests conducted is alternating plasticity.

In order to measure the severity of the cyclic plastic deformation (alternating plasticity) in these force-controlled cyclic tests and determine loading levels and inelastic responses (shakedown) that could be acceptable for design purposes, the evolution of hysteresis loop widths ($\delta\epsilon$) are monitored. This is because $\delta\epsilon$ correlates directly with the plastic work done per cycle (area within the hysteresis loop at each

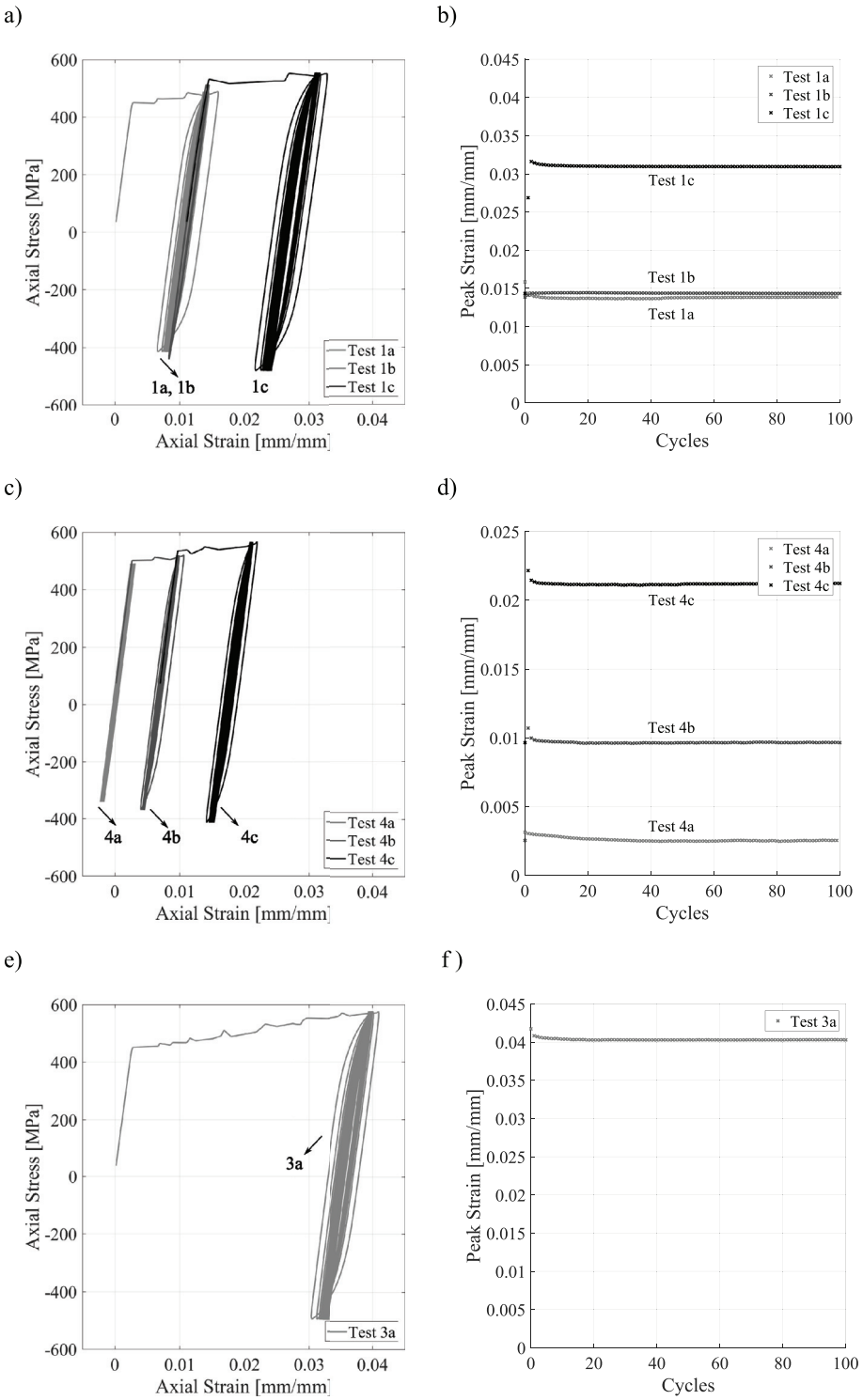

Fig. 6. Representative results for force-controlled cyclic tests at multiple stress amplitudes. Sample and test numbers are labeled according to Table 3.

cycle) (Hassan and Kyriakides, 1994). A hysteresis loop width of a cycle is calculated as the difference between the strain value obtained at the mean stress during loading and unloading of the cycle. Larger $\delta\epsilon$ values during cycling indicate alternating plasticity behavior is present that could result in failure of the material (LCF). When $\delta\epsilon$ decreases during cycling and approaches zero, the implication is that elastic behavior is being recovered, and the material approaches a safe shakedown state.

Fig. 7 shows examples of the evolution of the hysteresis loop width results calculated at the mean stress value for each cycle. Results from test #1a-c (solid line, multi-level), test #2a-c (dashed line, repetition of test #1a-c multi-level), and test #3a (dotted line, sample tested at the largest stress amplitude from test #2c, but without loading history) are compared in Fig. 7a. Similarly, results from test #7a-c (solid line, multi-level with compressive mean stress), test #8a-c (dashed line, repetition of test #7a-c), and test #9a (dotted line, sample tested at the largest stress amplitude from test #8c, but without loading history) are compared in Fig. 7b for the tests with compressive mean stress.

Based on Fig. 7, the width of the hysteresis loops decreases with load cycles. The results from the separate tests nearly coincide (solid, dashed, and dotted lines) with a maximum percent standard deviation

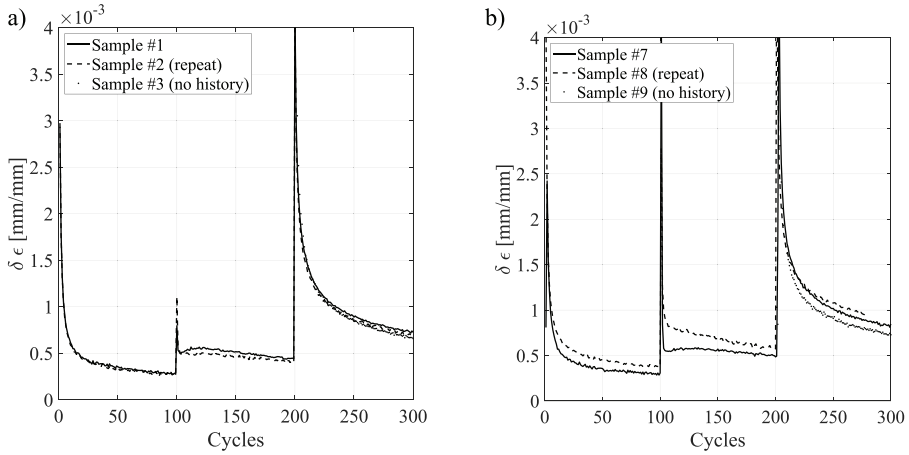

Fig. 7. Evolution of the hysteresis loop width during cycling.

of 10% in Fig. 7a (around cycle #120) and 20% (around cycle #110) in Fig. 7b. In Fig. 7a, only comparing tests with the same tensile mean stress and stress amplitude (#1c, #2c, and #3a), the maximum percent standard deviation was 5%. In Fig. 7b, only comparing tests with the same compressive mean stress and stress amplitude (#7c, #8c and #9a), the maximum percent standard deviation was 13%. Note that the maximum 20% standard deviation in Fig. 7b corresponds to an absolute strain difference of $6{\cdot}10^{-5}$ *mm/mm*. This value is negligible when compared to the absolute mean strain of 1.1% obtained in tests #7-8c. Thus, it is suggested that the tests are repeatable and the effect of the loading history on the results is negligible.

The same $\delta\epsilon$ analysis was done for all of the force-controlled cyclic tests listed in Table 3 to investigate the effect of the magnitude and sign of the mean stress on the evolution of the hysteresis loop widths with cycling (indicating the achievement of shakedown or alternating plasticity). Fig. 8a compares the evolution of $\delta\epsilon$ from tests with a mean stress of 72 MPa (test #4a-c with solid line, #5a-c with dashed line, and #6a-c with dotted line) with a sample tested under a mean stress of 36 MPa (test #1a-c, red crosses). It is observed that while a good agreement between the tests #4-6 with the same mean stress (72 MPa) was achieved, the final $\delta\epsilon$ values were 2–3 times larger when the mean stress was smaller by half (36 MPa). Similarly, Fig. 8b shows the hysteresis loop evolution with cycles for sample #10 (solid line), sample #11 (dashed line) and sample #7 (red crosses). The results show that, similarly to the tensile mean stress cases, the test under a smaller compressive mean stress by half (-36 MPa, sample #7) resulted in 2–3.5 times larger final hysteresis loop widths. Note that the maximum absolute stress applied in these seven tests was the same (554 MPa). This supports the idea that monitoring maximum stress alone is not sufficient for design considerations. Instead, the cyclic inelastic behavior, and in particular whether shakedown or alternating plasticity is effectively achieved, is determined by both the mean stress and stress amplitude. Furthermore, comparison of the plots in Figs. 8a and b shows that the evolution of hysteresis loop width is not affected by the sign of the mean stress. In this way, inelastic shakedown design may be equally considered for cycling with tensile and compressive mean stresses.

In Fig. 9, the cyclic inelastic behavior of each test is indicated using the load interaction diagram from Fig. 3b. Note that the linear elastic limit of the material is not visible in this diagram (i.e. all the loading combinations in the diagram would cause plastic deformation). The $\delta\epsilon$ analysis showed that the tests with large absolute mean stresses at 72 MPa (tests #4a, #5a, #6a, #10a, and #11a) have widths approaching zero (values around 1×10^{-5}) that may effectively reach shakedown. These shakedown tests are marked with blue circles in Fig. 9. Larger hysteresis loop widths were obtained from the rest of the tests listed in Table 3 indicating alternating plasticity behavior (marked with red squares). In this way, shakedown behavior is expected when the absolute mean stress is larger and the stress amplitude is smaller than tests #4-6a in the tensile mean stress region and tests #10-11a in the compressive mean stress region. This expected shakedown region is indicated by a shaded region in Fig. 9, however additional experiments are required for confirmation. Regardless, shakedown ocurred at maximum stress levels up to 1.4 times the linear elastic limit.

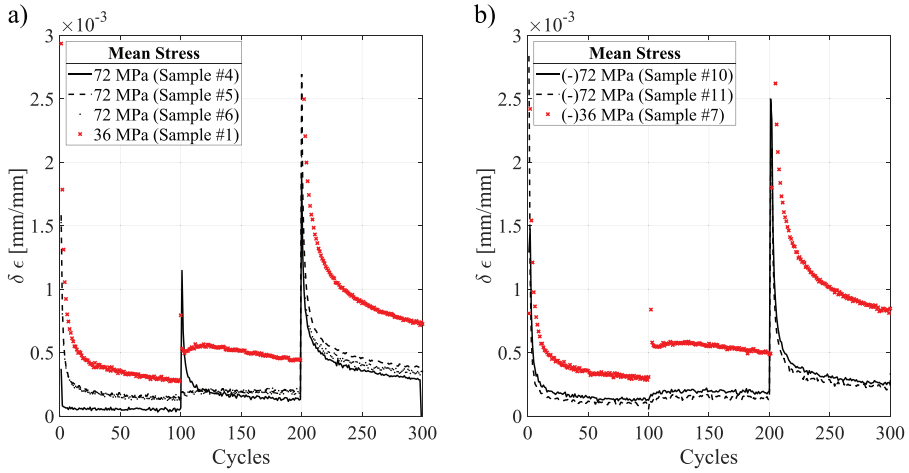

Fig. 8. Effect of mean stress on the hysteresis loop width results.

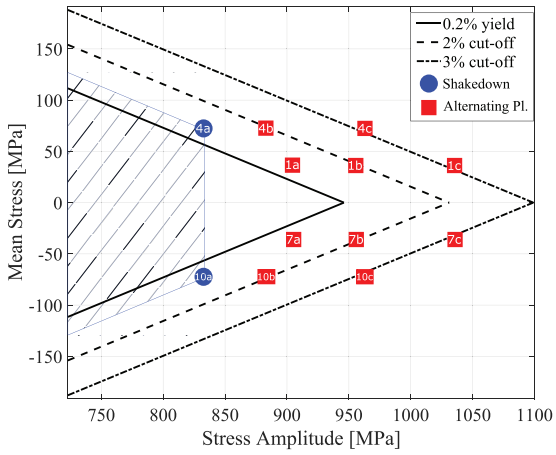

Fig. 9. Load-interaction diagram indicating cyclic elastoplastic behaviors.

While this is promising for inelastic design, DSA must also be considered and because of the large plastic strains that DSA may cause, in order to capitolize on shakedown, ways to suppress the DSA would be needed in order to reliably remain below allowable plastic strains. Unexpectedly, the strain levels reached in the first two levels overlapped for most of the multi-level force-controlled cyclic tests (an example of this is shown in Fig. 7a). Three distinct strain levels were visible only for sample #4 (Fig. 6c) and sample #8 (not shown). We believe that this is due to the DSA behavior observed during the initial loading to the maximum stress of each load level (a, b and c) in all of the cyclic tests (Fig. 3a, Table 3). In particular, sudden jumps in strain are seen due to DSA, creating a stair-like behavior in the plastic regime. As there are large post-yielding strain rates generated by the DSA mechanism, the strain value at the peak of the first cycle (at all load levels) varies greatly (even among repeat tests). These sudden jumps result in large strain values (that are otherwise not expected) at the maximum stress of the first test levels (level a, Fig. 3a). For instance, strain values of 0.3%, 1.4%, 1.5% and 1.6% were observed at 489 MPa in tests 1a-6a in Table 3, while based on the monotonic tests (Fig. 5), a strain value of 0.3% was expected. It is surmised that as a sample experiences large deformation in the first test level (level a) due to DSA, when loaded to the second level (level b), the strain does not noticeably increase. The result is the apparent overlapping of the hysteresis loops for the two levels. The stress-strain diagram in Fig. 6e shows the results of test #3a (Table 3) where the loading condition is identical to the test #1c but without any loading history. It is seen from this figure that the DSA is active until the maximum load in the first cycle is reached for test #3a. The maximum strain level is higher than test #1c although the stresses are identical. This is again believed to be due to the DSA.

5. Conclusions

The cyclic inelastic behavior of IN625 at 600˚C was investigated through force-controlled tests at various non-zero mean stresses and stress amplitudes. Hysteresis loop widths were monitored to explore the test conditions that result in shakedown behavior. The effect of dynamic strain aging on the macroscopic shakedown behavior in force-controlled tests was also examined. No cyclic accumulation of inelastic strain (ratchetting) was found and the samples showed either shakedown or alternating plasticity under the uniaxial loads considered in this study. Shakedown occurred at maximum stress levels up to 1.4 times the linear elastic limit.

Acknowledgment

This material is based, in part, upon work supported by the Air Force Office of Scientific Research (AFOSR) under award number FA9550-16-1-0438.

References

Algarni, M., Choi, Y., Bai, Y., 2017. A unified material model for multiaxial ductile fracture and extremely low cycle fatigue of inconel 718. Int J fatigue 96, 162–177.
Bui-Quoc, T., Gomuc, R., Biron, A., Nguyen, H., Masounave, J., 1988. Elevated temperature fatigue-creep behavior of nickel-base superalloy in 625. Low cycle fatigue. ASTM International.
Chaboche, J.-L., Lemaitre, J., 1990. Mechanics of solid materials. Cambridge University Press Cambridge.
Chatterjee, A., Sharma, G., Tewari, R., Chakravartty, J., 2015. Investigation of the dynamic strain aging and mechanical properties in alloy-625 with different microstructures. Metallurg Mater Trans A 46 (3), 1097–1107.
Donachie, M., Donachie, S., 2002. Superalloys a technical guide, asm international. Mater Soc Mater Park, Ohio.
Eiselstein, H., Tillack, D., 1991. The invention and definition of alloy 625. Superalloys 718 (625), 1–14.
Hassan, T., Kyriakides, S., 1994. Ratcheting of cyclically hardening and softening materials: i. uniaxial behavior. Int J Plast 10 (2), 149–184.
Heiser, W.H., Pratt, D.T., 1994. Hypersonic airbreathing propulsion. Aiaa.
Kim, I.S., Chaturvedi, M.C., 1987. Serrated flow in inconel 625. Trans Japan InstMetals 28 (3), 205–212.
Klock, R., Cesnik, C.E., 2015. Aerothermoelastic reduced-order model of a hypersonic vehicle. AIAA atmospheric flight mechanics conference. pp. 2711.
Maj, P., Zdunek, J., Mizera, J., Kurzydlowski, K., Sakowicz, B., Kaminski, M., 2017. Microstructure and strain-stress analysis of the dynamic strain aging in inconel 625 at high temperature. Metals Mater Int 23 (1), 54–67.
Mankins, W., Lamb, S., 1990. Nickel and nickel alloys. ASM International, Metals Handbook, Tenth Edition. 2, 428–445.
Nagesha, A., Parameswaran, P., Kumar, N., Sandhya, R., Mathew, M., 2012. Influence of re-solutionising treatment on the cyclic deformation behaviour of a service-exposed inconel® 625 superalloy. Mater High Temp 29 (1), 49–53.
de Oliveira, M.M., Couto, A.A., Almeida, G.F., Reis, D.A., de Lima, N.B., Baldan, R., 2019. Mechanical behavior of inconel 625 at elevated temperatures. Metals 9 (3), 301.
Park, S., Kim, K., Kim, H., 2007. Ratcheting behaviour and mean stress considerations in uniaxial low-cycle fatigue of inconel 718 at 649× c. Fatigue Fract Eng MaterStruct 30 (11), 1076–1083.
Rakowski, J.M., Stinner, C.P., Lipschutz, M., Montague, J.P., 2005. The use and performance of wrought 625 alloy in primary surface recuperators for gas turbine engines. Proc Superalloys 718, 625–706.
Shankar, V., Valsan, M., Rao, K.B.S., Mannan, S., 2004. Effects of temperature and strain rate on tensile properties and activation energy for dynamic strain aging in alloy 625. Metallurg Mater Trans A 35 (10), 3129–3139.
Shoemaker, L.E., 2005. Alloys 625 and 725: trends in properties and applications. Superalloys 718 (625), 409–418.
Standard, A., 2002. E466: Standard practice for conduction force controlled constant amplitude axial fatigue test of metallic materials, vol. 03.01. Annual Book of ASTM Standards, West Conshohocken.
Standard, A., 2004. E8. Standard test method for tension testing of metallic materials. West Conshohocken (USA): ASTM.
Standard, A., 2005. A370, Standard test methods and definitions for mechanical testing of steel products. West Conshohocken, PA: ASTM International.
Suave, L.M., Cormier, J., Bertheau, D., Villechaise, P., Soula, A., Hervier, Z., Hamon, F., 2016. High temperature low cycle fatigue properties of alloy 625. Mater Sci Eng: A 650, 161–170.
Thomas, C., Tait, P., 1994. The performance of alloy 625 in long-term intermediate temperature applications. IntJPressure VesselsPiping 59 (1–3), 41–49.
Vermaak, N., Boissier, M., Valdevit, L., McMeeking, R., 2018. Some graphical interpretations of melans theorem for shakedown design. Advances in Direct Methods for Materials and Structures. Springer, pp. 179–198.
Weichert, D., Ponter, A., 2014. A historical view on shakedown theory. The History of Theoretical, Material and Computational Mechanics-Mathematics Meets Mechanics and Engineering. Springer, pp. 169–193.
Zhu, S., Lei, Q., Wang, Q., 2017. Mean stress and ratcheting corrections in fatigue life prediction of metals. Fatigue Fract Eng MaterStruct 40 (9), 1343–1354.